JOURNAL OF BIOMOLECULAR STRUCTURE AND DYNAMICS
https://doi.org/10.1080/07391102.2024.2330706

Taylor & Francis
Taylor & Francis Group

Conformational analysis of lipid membrane mimetics modified with Aβ42 peptide by Raman spectroscopy and computer simulations

Kahramon Mamatkulov[a], Siarhei Zavatski[b], Yersultan Arynbek[a,c], Heba A. Esawii[a,d], Aliaksandr Burko[b], Hanna Bandarenka[b] and Grigory Arzumanyan[a]

[a]Laboratory of Neutron Physics, Sector of Raman Spectroscopy, Joint Institute for Nuclear Research, Dubna, Russia; [b]Applied Plasmonics Laboratory, Belarusian State University of Informatics and Radioelectronics, Minsk, Belarus; [c]Faculty of Physics and Technology, al-Farabi, Kazakh National University, Almaty, Kazakhstan; [d]Biophysics Department, Faculty of Science, Cairo University, Egypt

Communicated by Ramaswamy H. Sarma

ABSTRACT

Peptide-lipid interactions play an important role in maintaining the integrity and function of the cell membrane. Even slight changes in these interactions can induce the development of various diseases. Specifically, peptide misfolding and aggregation in the membrane is considered to be one of the triggers of Alzheimer's disease (AD), however its exact mechanism is still unclear. To this end, an increase of amyloid-beta (Aβ) peptide concentration in the human brain is widely accepted to gradually produce cytotoxic Aβ aggregates (plaques). These plaques initiate a sequence of pathogenic events ending up in observable symptoms of dementia. Understanding the mechanism of the Aβ interaction with cells is crucial for early detection and prevention of Alzheimer's disease. Hence, in this work, a comprehensive Raman analysis of the Aβ42 conformational dynamics in water and in liposomes and lipodiscs that mimic the membrane system is presented. The obtained results show that the secondary structure of Aβ42 in liposomes is dominated by the α–helix conformation, which remains stable over time. However, it comes as a surprise to reveal that the lipodisc environment induces the transformation of the Aβ42 secondary structure to a β-turn/random coil. Our Raman spectroscopy findings are supported with molecular dynamics (MD) and density functional theory (DFT) simulations, showing their good agreement.

ARTICLE HISTORY
Received 20 December 2023
Accepted 8 March 2024

KEYWORDS
Raman spectroscopy; MD; DFT; peptide secondary structure; conformational states

1. Introduction

Recent advances in the development of experimental and theoretical approaches for studying various molecular systems have largely accelerated new fundamental research. Considerable effort in this research area is being expended on the revealing interaction mechanisms between molecules and cell membranes as well as investigating their conformational transformations and structural changes. Amyloid-beta peptide derived from a transmembrane protein is one of the most intriguing molecular objects to understand its reciprocity with the cell membrane. Since the discovery of so-called 'neurofibrils' in the brain of patients suffering from dementia by Alois Alzheimer (Stelzmann et al., 1995) and further recognition of similar microscopic structural characteristics of amyloid proteins regardless of their different origins (Cohen & Calkins, 1959), the Aβ peptide has been under close attention of the scientific and medical community. A considerable attention upon seeking the effective AD early recognition and prevention methods is paid to dissolution or lessening the number of the existing fibrils. However, such an approach has never been favored to reduce the AD symptoms. Aβ is produced from proteolytic cleavage of amyloid precursor protein (APP) by β- and γ-secretase, which results in formation of a long amphiphilic Aβ peptide composed of 37–49 amino acid residues (Chen et al., 2017). These residues simultaneously exist in the human body, but Aβ40 is dominant in a healthy organism. After cleavage, the resulting monomeric Aβ peptides can leave the bilayer and come together to form oligomers, which are known to be unstable (Sakono & Zako, 2010). At the same time, if Aβ peptides do not leave the lipid bilayer after cleavage, the presence of monomeric peptides can influence the structure and dynamics, and hence the functionality of the cell membrane. It is generally accepted that the Aβ40 peptide does not negatively affect the human body, since it is free of amino acid residues that have pathogenic properties (Harrison et al., 2007). On the contrary, Aβ42 peptides are extremely toxic and considered to be a hallmark of Alzheimer's disease (Harrison et al., 2007). Such peptides accumulate in the brain, form β-folds, aggregate to fibrils, and subsequently turn into amyloid plaques.

It is believed that the fibrillization process occurs as a result of Aβ peptide and cell membrane interaction in the brain (Straub & Thirumalai, 2014). That is why the

CONTACT Hanna Bandarenka h.bandarenka@bsuir.by Applied Plasmonics Laboratory, Belarusian State University of Informatics and Radioelectronics, Minsk, Belarus; Grigory Arzumanyan arzuman@jinr.ru Laboratory of Neutron Physics, Sector of Raman Spectroscopy, Joint Institute for Nuclear Research, Dubna, Russia

Supplemental data for this article can be accessed online at https://doi.org/10.1080/07391102.2024.2330706.

relationship between the membrane and Aβ peptides has been studied quite extensively (Picone et al., 2020). As of today, it is generally accepted that Aβ peptide can interact with the phospholipid membrane in two ways (Niu et al., 2018). The first one considers insertion of the Aβ peptide into the membrane leading to its permeabilization and the cell death. The other type of interaction goes *via* binding Aβ peptide on the lipid layer surface, which causes compression and thinning the cell membrane. It should be noted that the binding of α-helical structure onto the membrane is more typical at high lipid/peptide ratios while lower ratios result in an oligomer with a trans-membrane pore-like structure (Wong et al., 2009). In addition to the lipid/protein ratio, the surface charge of the membrane also affects the Aβ peptide membrane interaction and can provoke a transformation of the peptide secondary structure (Bokvist et al., 2004). In more detail, a negatively charged membrane facilitates electrostatic binding of Aβ peptide through positively charged sites. As the membrane surface charge increases, hydrophobic effects play a dominant role in determining the interaction character when the hydrophobic segment of the peptide is incorporated into the membrane.

Despite numerous Aβ-cell interaction mechanisms have already been deciphered to some degree, capturing the moment of the Aβ release from the cell membrane and understanding their conformation transformations are still unclear. Overcoming this issue may be a small yet important step towards shedding the light on such complex bioorganic processes. A long-term objective is to yield a full Aβ–cell interaction model that would open the door to AD control and prevention.

Different membrane mimetics such as bicelles, micelles, liposomes, and nanodiscs have been reported to study the structure of transmembrane proteins in experiments and theoretical calculations (Majeed et al., 2021). The use of a copolymer of styrene and maleic acid (SMA) is known as one of the novel methods for isolating membrane proteins (Dörr et al., 2016). This amphipathic copolymer can be incorporated into cell membranes and easily disrupt them. As a result, discoid membrane fragments surrounded by a copolymer belt are produced with a typical size of 10–40 nm. These particles are known as SMALP (SMA lipid particles) or lipodiscs (Craig et al., 2016; Wheatley et al., 2016).

It is believed that lipodiscs preserve native membrane-protein complexes for structure-function analysis (Chorev & Robinson, 2020; Vargas et al., 2015). Hence, in our experiment, SMA is utilized for purification and study of membrane proteins while preserving the biological lipid environment.

Modern computer modeling methods fruitfully contribute to an in-depth understanding of the interaction mechanisms of Aβ with cells. Such methods can gain insights into molecular processes at the microscopic level, which is rather difficult or completely impossible to do experimentally.

Molecular dynamics is one of the most powerful theoretical tools that is effectively used to simulate physical and biological systems (Allen & Tildesley, 1989). MD provides high spatiotemporal resolution and enables simulation of atomic and molecular scale processes that occur during negligibly short times from tens to hundreds of nanoseconds. This method facilitates versatile characterization of molecular systems, which can hardly be achieved with other theoretical techniques (Berkowitz, 2009; Mezei & Jedlovszky, 2007; H. L. Scott, 2002; Vigh et al., 2005). In addition, MD is a common choice for investigating the process of peptides embedding into biological membranes (Efremov et al., 2012; Gumbart et al., 2005; Khandelia et al., 2008; Killian & Nyholm, 2006). It should be noted that the exact mechanism of the peptide-membrane complex formation remains unclear. To this end, studying the interaction of peptides with membranes using all-atom molecular modeling methods is relevant from both fundamental and applied perspectives.

Despite the proven robustness of MD for dynamic and conformational structure investigation of bioorganic systems, its key limitation is the fact that these calculations are based on classical mechanics. Indeed, such important molecular processes as polarization, chemical reactions, and molecular vibrations cannot be explained accurately by laws of classical mechanics. Simulation of these properties requires precise description of a system electronic structure. In the classical MD formulation, the effect of electrons is usually averaged out in terms of introduction of specific force fields. These forces are usually defined empirically or in terms of quantum mechanical calculations (Leach, 2001). However, the representation of only one state of the system (usually ground state) is possible by these approaches. Therefore, when a more detailed system description or simulation of vibrational dynamics is required, quantum mechanical methods, such as density functional theory (Born & Oppenheimer, 1927; Burke, 2012; Sholl & Steckel, 2009), are utilized.

DFT approach is a computer simulation method for determination of an electron ground state energy in the considered many-atom system. However, owing to the complexity of the method, the calculation of dynamic systems containing 500–1000 atoms remains challenging in terms of computational costs required to solve the system of Kohn-Sham equations (Kohn & Sham, 1965). Although the calculation of a ground state energy for such relatively large systems as peptides, proteins, and DNA is currently feasible (Cole & Hine, 2016), the computational time required to find their vibrational dynamics drastically grows with the number of atoms. Calculations may last for months or even years depending on the available computing power because—in addition to the total electron energy—the simulation of molecule vibrations requires finding first (for simulation infrared absorption spectra) or second (for simulation of Raman scattering spectra) energy derivatives (Herrmann & Reiher, 2006). Therefore, the development of strategies that can reduce the computational time needed to explore electronic properties of large substances has recently attracted a great attention. In these methods, the big molecule is split into one or several smaller entities that are subjected to a full DFT characterization, while the remaining part is fixed. For example, utilizing such an approach, Berhanu et al. (Berhanu et al., 2010) have calculated Raman spectra for hexapeptides of glutamic acid and lysine in three different conformations. In another study, the authors have calculated full electronic energy of Aβ (28–35) and its mutated forms in several

different conformations. A good agreement between calculations and experiments has been reported. Marino et al. have also investigated structural and energetic transformations of Aβ after addition of Cu^{2+} and Zn^{2+} ions to reveal their role in formation of toxic Aβ plaques (Marino et al., 2010).

The proposed strategies to reduce computational time required to compute electronic energy of macromolecules by DFT are useful for investigation of different molecular conformations. However, the accuracy of IR or Raman spectra calculated this way is uncertain because only part of the molecule electronic structure is fully simulated by DFT. This problem has been recently addressed by P. Bour and colleagues by proposing a new fragmentation technique named Cartesian Tensor Transfer Method (CTTM) (Bouř et al., 1997; Collins & Bettens, 2015; Gordon et al., 2012; Kessler et al., 2015; Raghavachari & Saha, 2015). It relies on the same principle of full DFT calculations for molecule fragments but introduces additional steps of combining the obtained results and translating them back onto the big molecule. In this method, DFT calculations of first and second energy derivatives are performed for small molecular parts, while the Hessian matrix required for vibrational spectrum calculations is constructed from these parts for the entire molecule, reducing the computational time significantly. The CTTM approach has been applied for Raman (Bouř et al., 2001, 2000), IR (Bouř et al., 2000; Grahnen et al., 2010; R. Huang et al., 2007; J. Kubelka & Keiderling, 2001; Mazaleyrat et al., 2003), and Raman optical activity (Hudecová et al., 2010; Kapitán et al., 2006, 2008; Sebek et al., 2009; Zhu et al., 2008) spectrum calculations of various substances, including insulin (Yamamoto et al., 2012), β-peptide (Kapitán et al., 2008), valinomycin (Yamamoto et al., 2010, 2011), bovine α-lactalbumin, concavalin-A, lysozyme from chicken egg white, human lysozyme, human serum albumin (Kessler et al., 2015), and other polypeptides (Mensch et al., 2019). This broad application range along with performed reliability tests (Bieler et al., 2011) and accessibility of a computer code for the public (Neese, 2012; Neese et al., 2020) makes the CTTM method an ideal candidate for investigation of bioorganic macromolecule vibrational properties by DFT.

We thus study molecular systems based on model cell membranes and Aβ42 by Raman scattering spectroscopy, MD and DFT simulations to reveal their conformational transformations. A schematic representation of this approach is depicted in Figure 1.

Firstly, we perform a Raman spectroscopy study of native Aβ42 in an aqueous environment, a 1,2-dimyristoyl-sn-glycero-3-phosphocholine (DMPC) liposome, and a SMA/DMPC lipodisc. Specifically, we record the time evolution of conformation-sensitive Raman vibrational bands, namely peptide Amide I region, to reveal the degree and kinetics of the molecular structure transformation. Next, we launch massive MD simulations for the same molecular systems to elucidate the Aβ42 structure evolution from a theoretical point of view. Simulation results obtained this way are then correlated with experimental Raman data acquired at the previous study step. Finally, we conduct the first principle calculations of Raman spectra utilizing the DFT approach augmented by the CTTM method (Bouř et al., 1997). The input molecular structures of Aβ42 for DFT are those obtained after MD simulations. Consequently, by sequentially linking all study steps together, we produce a solid and correlated multi-level theoretical dataset to support our experimental observation of Aβ42 conformation transformations in various environments.

2. Methods and experiments

2.1. Synthesis of liposomes (DMPC) and lipodiscs

2.1.1. Liposomes

Phospholipid powder, 1,2-dimyristoyl-sn-glycero-3-phosphocholine (DMPC), (Avanti Polar Lipids, USA), and chloroform (Sigma Aldrich, USA) were used for liposome synthesis. The phospholipid powder was dissolved in chloroform at a concentration of 3.4 mg/mL. Next, 20 µL of the prepared solution was applied dropwise to the conductive side of an indium tin oxide (ITO) glass slide. The solvent was subsequently evaporated under vacuum for 60 min. The obtained dry phospholipid layer was then surrounded by a 16 mm rubber O-ring, redispersed in the 250 µl drop of double distilled water, and placed in the electroforming chamber of the Vesicle Prep Pro device (VPP, Nanion Technologies GmbH, Germany). Before launching liposome synthesis, the O-ring was covered by a second ITO glass slide. The VPP device was run at a voltage of 3 V and a frequency of 5 Hz for 60 min at 37 °C. Finally, synthesized liposomes were carefully transferred into an Eppendorf tube and stored at room temperature before use.

2.1.2. Lipodiscs

Lipodiscs were synthesized by adding aqueous solution of the SMA copolymer (3.4 mg/ml, Sigma Aldrich, USA) to the liposome suspension, obtaining the following SMA/DMPC molar ratios: 0.16, 0.32, 0.64, and 1.28. In accordance with the method outlined in Zhang et al. (2015), the mixtures were allowed to stabilize for 16 h at room temperature to create lipodiscs. The lipodisc solution was extruded by filtering *via* a 50 nm pore membrane filter (Avanti Polar Lipids, USA) for 11 times.

2.2. Synthesis of liposome/peptide and lipodisc/peptide systems

2.2.1. Liposome/peptide systems

First, a solution of 1 mg/mL of Aβ42 (Abbiotec, USA) in double distilled water was prepared. Next, the same electroformation technique was used to produce liposome/peptide systems, adding 250 µL of Aβ42 solution to a vacuum-dried phospholipid on an ITO glass slide instead of water. The peptide concentration within the liposome/peptide system was 3% molar.

2.2.2. Lipodisc/peptide systems

A lipodisc/peptide system was obtained by introducing SMA with concentration of 3.4 mg/ml to the liposome/peptide

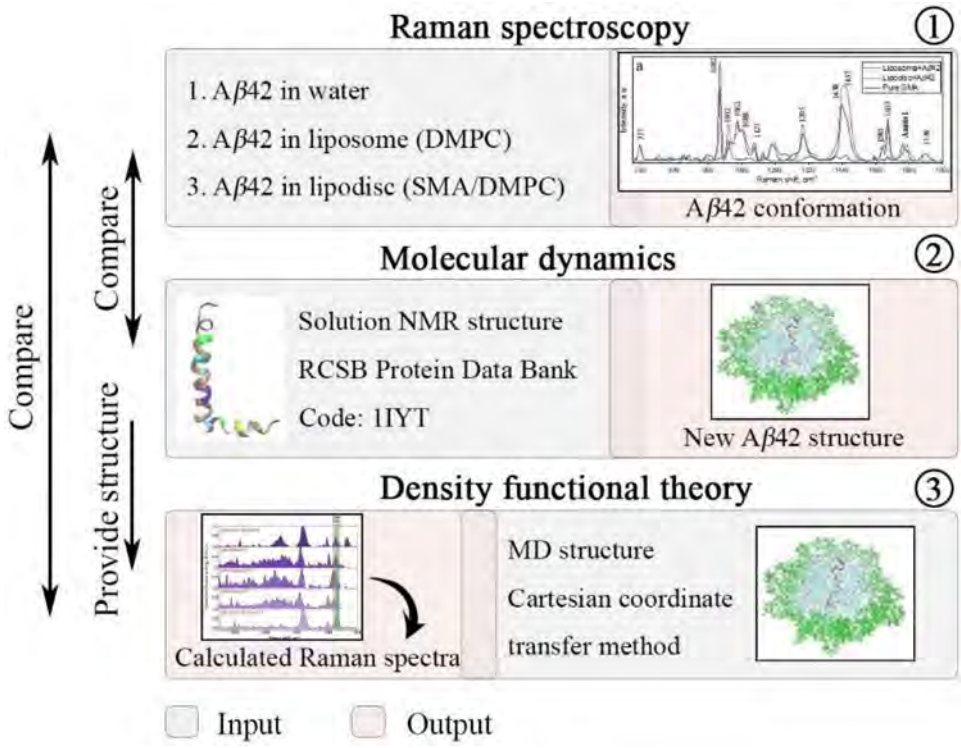

Figure 1. Schematic representation of model cell membrane and Aβ42 systems studied by Raman scattering spectroscopy, MD and DFT simulations.

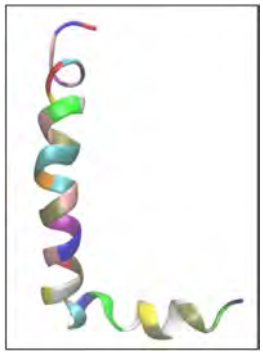

Figure 2. PDB structure of 1IYT.

suspension, at the molar ratio of SMA/DMPC equal to 1.28. The mixture was allowed to stabilize at room temperature for 16 h before being passed through an extruder 11 times using a 50 nm pore diameter membrane filter.

2.3. Molecular dynamics

CHARMM-GUI Membrane Builder (Jo et al., 2007, 2008, 2009, 2014; Wu et al., 2014) was used to build liposome and lipodisc systems for the following MD simulations. A molecular structure of Aβ42 was taken from RCSB Protein Data Bank (1IYT, PDB, http://www.rcsb.org/) (Berman et al., 2000; Crescenzi et al., 2002) (Figure 2).

Additional simulation packages, such as VMD, Chimera, and Pymol were used for the visualization and timeline analysis of the liposome and lipodisc systems (DeLano, 2020; Humphrey et al., 1996; Pettersen et al., 2004).

GROMACS 5.1.3 package (Abraham et al., 2015) with CHARMM36m force field (J. Huang et al., 2016) was utilized for the MD simulation of liposome and lipodisc systems. Aβ42 was embedded into a base membrane system consisting of 114 DMPC molecules. To build an SMA polymer and produce configuration of a lipodisc, we used an additional python script (https://github.com/Tarasovk49/2018_lipodisk_md/).

MD simulations were performed at an ambient temperature of 294.15 K. Aβ42 was solvated in a cubic box of TIP3P water molecules, where each side of the box is 12 nm. To neutralize the system total charge, counter-ions (Na^+ and Cl^-) were added to the box, whereas the protonation state of the peptide was −3.

The energy of the system was minimized using 5,000 steps of the steepest descent algorithm. The electrostatics calculations were performed by the Ewald method with a cut-off radius of 12 Å. The periodic boundary conditions were used in all three dimensions. In the system balancing step, we have used a Berendsen thermostat at a temperature of 294.15 K for the NVT and NPT ensembles, as well as a semi-isotropic Berendsen barostat for a pressure balancing at 1 bar for the NPT ensemble.

The system was equilibrated in two phases. In the first phase, equilibration was conducted for 0.375 ns under an NVT ensemble (constant number of particles, volume, and temperature). The temperature was maintained with a V-rescale thermostat. In the second phase, equilibration was conducted for 1.5 ns under an NPT ensemble (constant number of particles, pressure, and temperature). Pressure was maintained at 1 bar using a Parrinello–Rahman barostat. Bond lengths were constrained using the linear constraint solver (LINCS) algorithm. Short-range interactions were truncated at 14 Å and long-range ones were handled with the particle mesh Ewald (PME) method.

Finally, the production simulations were carried out in the NPT ensemble with a Nose-Hoover thermostat at 294.15 K and a Parrinello-Rahman barostat at 1 bar for 100 ns. The temperature and pressure of the entire system (membrane and water solvent) were connected independently to each other. All simulations were carried out assuming the full hydration state by introducing more than 40 water molecules per lipid.

2.4. Density functional theory

All quantum-mechanical calculations were performed by the DFT method implemented in ORCA 5.0.1 software package (Neese, 2012). The chosen molecular structures of Aβ42 are visualized *via* Avogadro software and depicted in Figure 3. The structure displayed in Figure 3(a) was obtained from the NMR structure 6SZF taken from PDB. Meanwhile, the structures in Figure 3(b,c) were generated through our MD simulation of the Aβ42 interaction with liposomes and lipodiscs, respectively. PDB geometry was additionally corrected using the tleap module of Amber software (Case et al., 2005) to include missed heavy and hydrogen atoms.

Following the procedure described elsewhere (Kessler et al., 2015), the chosen Aβ42 structures were cut into 39 small fragments, each consisting of 4 amide (3 amino acid) residues (Figure 4). The ends of polypeptide fragments were terminated by methyl groups, forming CH3–NH–CO– … and … –NH–CO–CH_3 connections from both sides. Each subsequent fragment of Aβ42 was constructed with a shift by one amide residue relative to the previous fragment.

The normal mode method (Bouř & Keiderling, 2002) was used to optimize the fragment geometries. This method allows for the complete relaxation of the most critical vibrational modes while keeping the overall molecular structure relatively unperturbed. As a result, the normal mode method helps to calculate the Raman spectra without significantly compromising the correlation of molecular conformation with experiments or MD simulations.

The initial guess of the Hessian matrix is required before starting the normal mode optimization. DFT calculations were performed using a low theoretical level (B3LYP (Becke, 1993; Lee et al., 1988; Parr, 1980)/STO-3G) to make this guess. The resulting matrix was then utilized to search for the minimum system energy on a higher DFT level (B3PW91 (Perdew et al., 1996)/6-31++G**) while keeping vibration modes fixed within the −100 - 300 cm^{-1} range. This range corresponds to the skeletal (main polypeptide chain) vibrations of the molecule. All DFT calculations were conducted by accounting for the effect of an environment with the help of a polarizable continuum model (PCM) (Klamt et al., 1998; Mennucci et al., 2011) and water as a solvent.

To calculate the Raman spectrum of the molecule, the mass-weighted Hessian matrix and electrical dipolar-electrical dipolar polarization tensor were obtained for each fragment utilizing the same DFT parameters as on the step of the normal mode optimization. They were next transferred on the initial Aβ42 molecule structure by the CCTM method (Bouř et al., 1997), producing one composite matrix and tensor.

Next, the obtained molecular properties were utilized to calculate vibrational frequencies and Raman activities (Barron, 2004; Nafie, 2011; Polavarapu, 1990). We applied the orca_vib supplementary code for this purpose (Neese, 2012). Finally, the realistic Raman spectrum for Aβ42 was acquired with orca_mapspc supplementary code. The Voight function

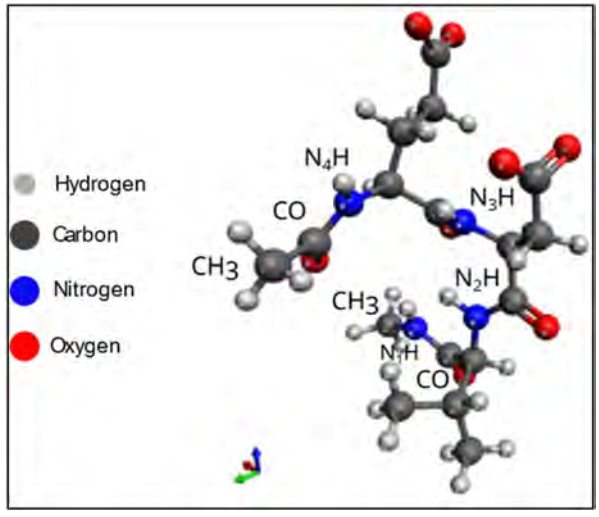

Figure 4. Example of Aβ42 fragment utilized in CTTM calculations.

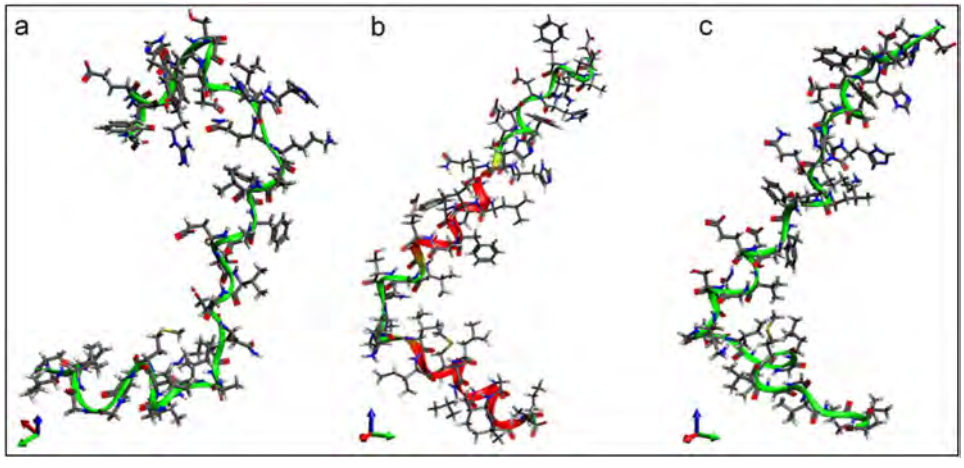

Figure 3. Aβ42 structure acquired from (a) PDB database (6SZF) and after MD simulation of interaction with (b) liposome and (c) lipodisc.

and peak full-width half-maximum of 10 cm^{-1} were selected for vibrational modes convolution. In addition, we adjusted the vibrational frequencies by a factor of 0.97 to avoid the common overestimation error (https://cccbdb.nist.gov/vibscalejustx.asp). This error arises from various DFT approximations, such as the harmonic oscillator model, calculations at absolute zero temperature, the use of an unknown form of exchange-correlation energy functional, and a finite set of basis functions.

2.5. Raman spectroscopy and instrumentation

In this work, a scanning confocal laser microspectrometer 'Confotec CARS' (SOL Instruments LLC, Belarus) combined with a NIKON TE2000-E inverted microscope was used for all Raman measurements. We utilized a diode-pumped single-frequency laser at a wavelength of 532 nm with adjustable output power (model SLM-417-20) for sample excitation. The laser beam was focused on the sample to a spot with a diameter of ~1 μm using an Olympus 40× (NA-0.6) objective. Samples were placed on a motorized stage (Prior Scientific, H117TE).

All Raman spectra were collected in a backscattering geometry and dispersed by a MS520 monochromator equipped with a 600 gr/mm diffraction grating. Spectra were recorded by a Peltier-cooled charge-coupled device (CCD) camera (ProScan HS-101H).

3. Results and discussion

3.1. Raman spectroscopy measurements

3.1.1. Native Aβ42 in water

The Raman spectra of Aβ42 were collected in water over 24 h, with measurements taken every two hours during the first five hours. The purpose was to study the kinetics of alternating the Amide I band (1620–1690) cm^{-1} positions, as shown in Figure 5(a,b). This spectral region is sensitive to changes in the peptide's secondary structure (Bunaciu et al., 2015). Figure 5b shows that for the first five hours, α-helix (1657 cm^{-1}) is the dominant conformation of Aβ42, as indicated by the normalized Raman frequencies. However, significant changes in the secondary structure of the peptide were observed in Raman spectra measured 24 h later. The spectral marker for α-helices at 1657 cm^{-1} was less pronounced compared to the 1671 cm^{-1} Raman band, indicating the dominance of β-turn/random coil conformation in the secondary structure. This transformation can be caused by partial peptide denaturation due to adsorption to the air-water interface (D'Imprima et al., 2019) and attributed to the formation of Aβ aggregates, which are the precursor to Alzheimer's disease (Harrison et al., 2007).

3.1.2. Aβ42 in the presence of liposomes

Raman spectra of the Aβ42/liposome system collected for two days are depicted in Figure 6(a,b). The following Raman bands are observed in the spectral fingerprint region of phospholipids: C–N oscillation of the phospholipid headgroup (717 cm^{-1}), C–C backbone stretching (1060–1180 cm^{-1}), CH_3–twisting (1250–1300 cm^{-1}), and CH_2 scissor oscillations (1400–1500 cm^{-1}). The vibrational modes at 1062 and 1127 cm^{-1} are due to asymmetric and symmetric C-C vibrations of the trans conformer in the phospholipid tail, while the 1088 cm^{-1} vibrational band corresponds to vibrations of single gauche defects and/or different gauche isomers (Bunow & Levin, 1977; Bush et al., 1980; Fasanella et al., 2018; Spiker & Levin, 1975). Raman frequencies at 1295, 1437, and 1458 cm^{-1} are evident in the spectra of both the peptide and phospholipid, while the C = O stretching mode at 1656 cm^{-1} is observed only for Aβ42 in the Amide I region.

Figure 6(b) shows that the spectral weight ratio of α-helix (1656 cm^{-1}) to β-turn/random coil (1671 cm^{-1}) does not significantly change after 48 h of exposure. This suggests the conformational stability of the peptide's secondary structure in the liposome/peptide environment. The temporal stability of α-helical secondary structure in the lipid bilayer environment is confirmed by our MD simulation and reported previously by another group (Poojari et al., 2013). These results suggest that the liposome/peptide system formed in this work closely resembles the natural state.

Raman measurements were then conducted for lipodiscs both in the presence and without Aβ42. Figure 7(a,b) shows typical spectra of lipodiscs in the absence of Aβ42 for four different SMA/DMPC molar ratios: 0.16, 0.32, 0.64, and 1.28. The normalized spectra in the 1040–1140 cm^{-1} region demonstrate the intensity variation of vibrational bands associated with the trans (1062 and 1127) cm^{-1} and gauche 1088 cm^{-1} conformation of the phospholipid (Figure 7b).

Figure 7(b) also shows that the increase of the SMA/DMPC molar ratio produces a higher intensity of 1127 cm^{-1} vibrational band of the trans component. This observation is in accordance with our previous studies (Zavatski et al., 2022), and suggests ordering in the carboxyl chains of the phospholipid bilayer. Meanwhile, the intensity of the gauche conformation decreases with increasing SMA/DMPC ratio. Quantitative estimates of the effect of the SMA/DMPC ratio on the degree of ordering of the phospholipid bilayer are summarized in Table 1. The ratios were obtained by fitting spectra using the Gaussian function.

Figure 8 shows the Raman spectra of the lipodisc/peptide system measured at day 1, day 2, and day 3 after formation. It can be seen from 8(b) that the system is as stable as the liposome/peptide system, but the Amide I band region is dominated by the β-turn/random coil conformation at 1671 cm^{-1}.

To illustrate the comparison of the obtained Raman spectra, Figure 9(a) shows the spectra of the liposome/peptide, lipodisc/peptide systems, and SMA.

The most intense and narrowest Raman line at 1002 cm^{-1} corresponds to the breathing mode of the phenylalanine benzene ring and the copolymer. Similarly, to the liposome/peptide system, we also analyze the spectral region of the Amide I band in the lipodisc/peptide system (red line in Figure 8a).

Figures 9(b,c) show the deconvolved spectra in the Amide I region for the liposome/peptide and lipodisc/peptide systems. These figures suggest the dominance of the α-helix

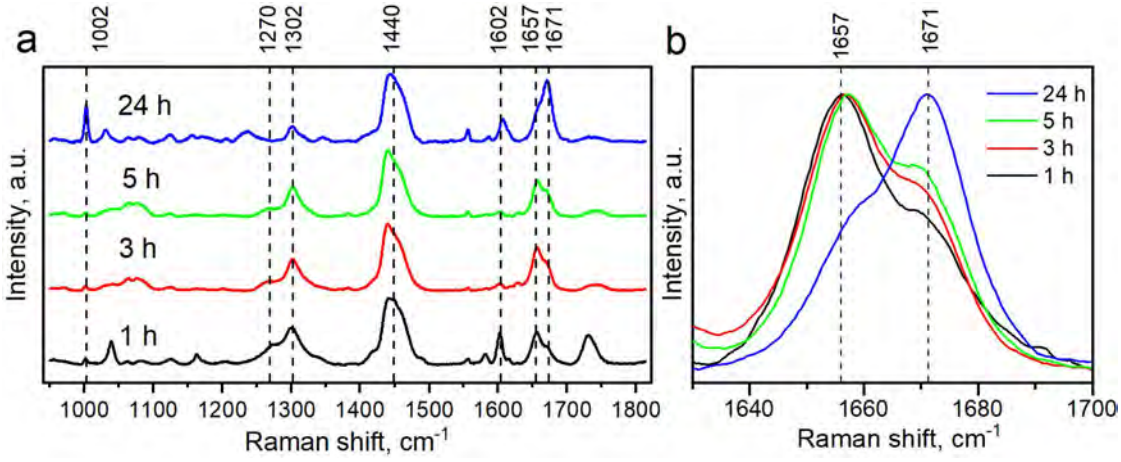

Figure 5. (a) Raman spectra of the peptide in aqueous medium by hours, and (b) normalized spectra of the peptide in the Amide I region.

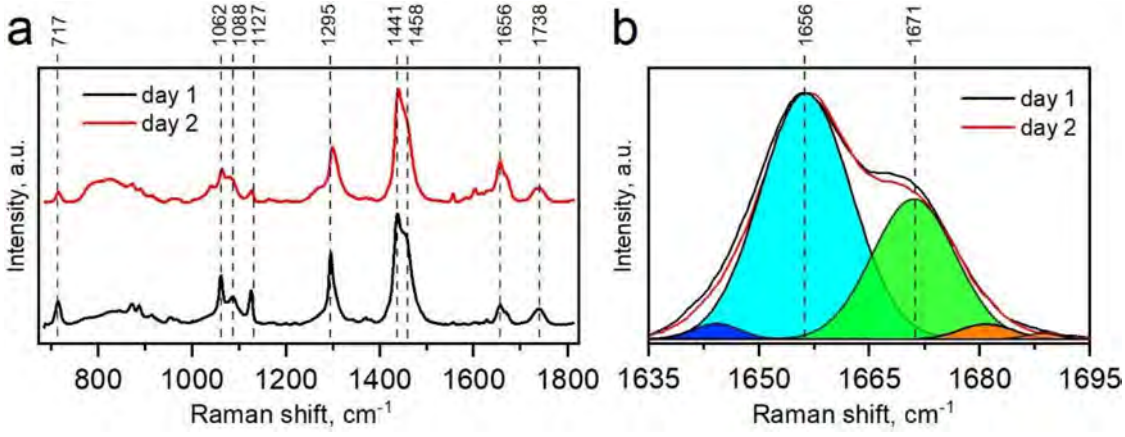

Figure 6. (a) Raman spectra of the liposome/peptide system by day, (b) normalized spectra of the peptide in the Amide I region.

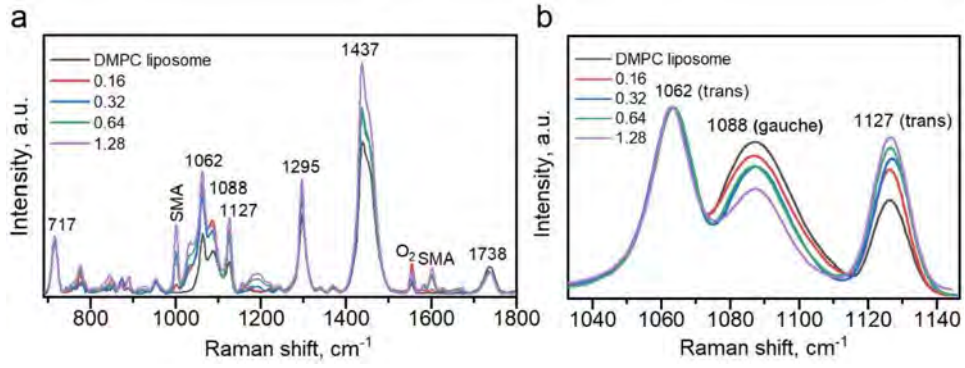

Figure 7. (a) Raman spectra of lipodiscs in the absence of peptide with different molar ratios of SMA/DMPC, and (b) normalized spectra in the range (1040–1140) cm^{-1} after subtraction of the SMA copolymer spectrum.

Table 1. Spectral weight ratios of trans/gauche conformations in lipodiscs in the absence of peptides as a function of SMA/DMPC molar concentration.

		SMA/DMPC molar ratio:			
Trans/gauche band ratio	Liposome DMPC	0.16	0.32	0.64	1.28
$I_{1062/1088}$	0.76 ± 0.07	1.10 ± 0.11	1.16 ± 0.11	1.03 ± 0.1	1.39 ± 0.13
$I_{1127/1088}$	0.23 ± 0.02	0.37 ± 0.03	0.53 ± 0.05	0.52 ± 0.05	0.75 ± 0.07

fraction in the liposome/peptide system with the calculated spectral weight of 62.3%, and of the β-turn/random coil fraction in the lipodisc/peptide system with the calculated spectral weight of 72.1%.

We thus may assume that the copolymer girdling the lipodisc/peptide system leads to the ordering of the carboxyl chains in the bilayer, and thus affects the secondary structure of the Aβ42 peptide. This assumption is also

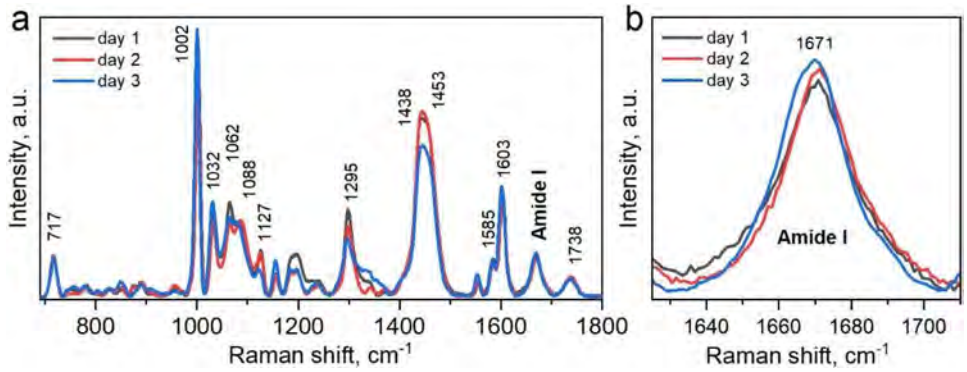

Figure 8. (a) Raman spectra of the lipodisc/peptide system by day, (b) spectra of the peptide in the Amide I region.

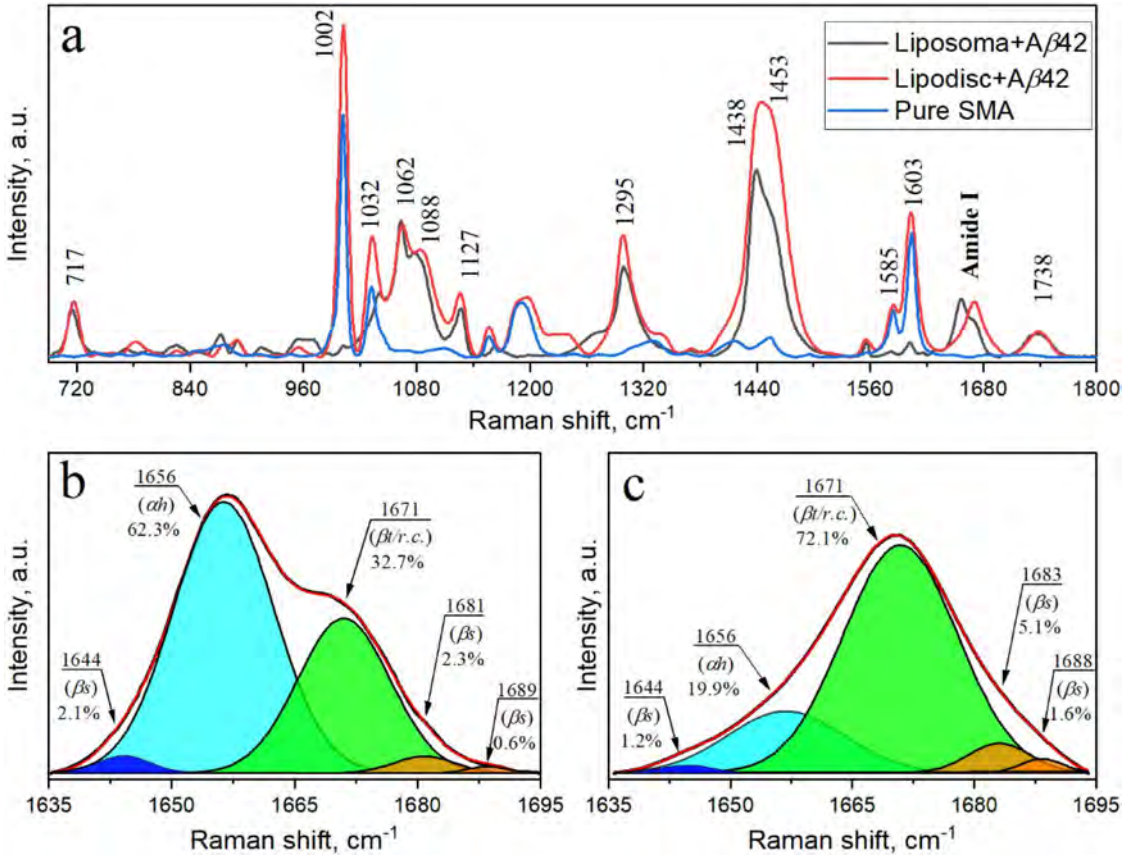

Figure 9. (a) Raman spectra of SMA (blue line), liposome/peptide (black line), and lipodisc/peptide (red line) with a molar ratio (SMA/DMPC) of 1.28. Deconvolved Raman spectra of the peptide in the Amide I region: (b) in liposome/peptide, (c) in lipodisc/peptide. Red line - fitted curve, filled areas - deconvolved spectra by Gaussian function. αh – α-helix, $\beta t/r.c.$ – β-turn/random coil, βs – β-strand.

supported by our MD and DFT simulation results presented further.

3.2. Aβ42 Conformational change due to the surroundings

We also simulate liposome/peptide and lipodisc/peptide systems by the MD approach. The corresponding structures of the Aβ42 peptide embedded in the liposome and in the lipodisc are demonstrated in Figure 10 (a,b) and Figure 10 (c,d), respectively.

Figure 10(a) shows the structure of peptide before the equilibration step, which is mainly in the α-helix conformation with a small fraction of β-turn conformation. The corresponding data are summarized in Table 2.

Figure 10(b) shows the simulation results for the peptide embedded in the liposome after the equilibration process. These results indicate that the liposome/peptide system preserves the α-helical conformational structure. Figure 10(d) shows the simulation results for the peptide embedded in the lipodisc after the equilibration process. In this case, we observe the transformation of the peptide secondary structure dominated by the β-turn conformer. The results from both simulated systems are in a good agreement with the measured Raman spectra (Figures 6, 8, and 9).

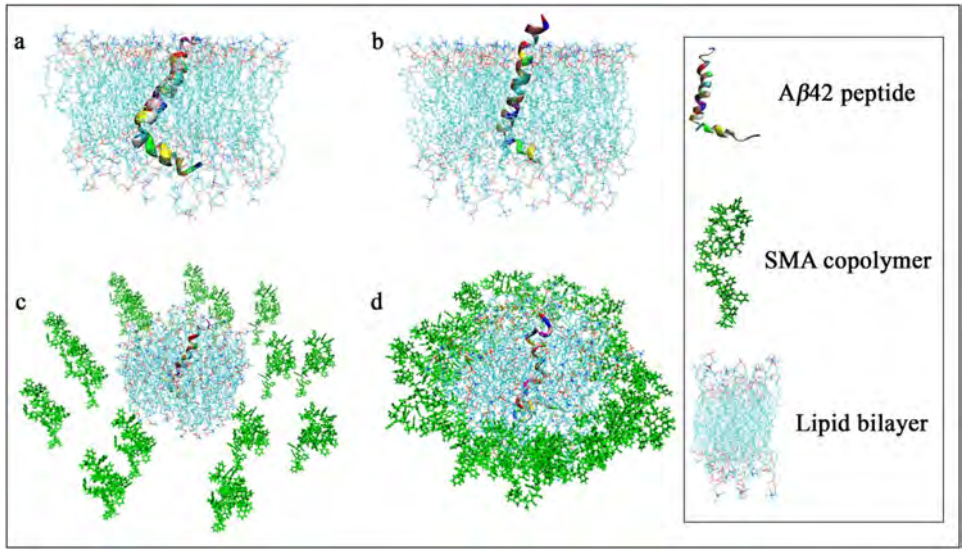

Figure 10. 3D structure of 1IYT Aβ42 peptide embedded in liposome and lipodisc obtained using Charmm Gui membrane builder (water and ions excluded for clarity): (a,b) liposome/peptide, (c,d) lipodisc/peptide, respectively. (a,c) - before, and (b,d) - after equilibration step in the MD simulation.

Table 2. Secondary structures of amino acid residues of peptide Aβ42 in % ratio.

Secondary structure	Pedtide's initial structure, %	Peptide in liposome, %	Peptide in lipodisc, %
Random coil	4.76	19.61	12.02
ß-turn	21.42	7.94	71.4
α-helix	73.81	69.93	14.2
others	–	2.52	2.38

3.3. Theoretical Raman spectra for Aβ42 in different conformations

3.3.1. CCTM method verification

Before proceeding with DFT calculations of Aβ42 Raman spectra, we verify our implementation of CTTM method (please see SI). Similarly to the previously established procedures (Bieler et al., 2011; Bouř et al., 1997), we take a N-methylacetamide (NMA) trimer as a test molecule (Figure S1). We next partition this molecule into two identical fragments, each containing two N atoms (N_1/N_2 or N_2/N_3, respectively) and methyl groups CH_3 from both ends of the molecule (Figure S2). The Raman spectrum for the NMA trimmer is calculated by launching a full DFT simulation with the parameters indicated in the experimental section. This spectrum is next compared to those obtained by CTTM approach, where geometry of NMA fragments is first optimized by a normal mode method (Bouř & Keiderling, 2002) and then subjected to the DFT simulation. Finally, DFT simulated electronic properties of fragments are transferred onto the geometry of the NMA trimmer by CTTM approach.

3.3.2. CCTM calculations for isolated Aβ42

Figure 11 shows CTTM simulated Raman spectra for different conformations of Aβ42, including experimental results presented previously (Figure 4): experimental Raman spectrum of Aβ42 immediately after dissolution in water; simulated Raman spectrum of Aβ42 with the structure obtained from the PDB database; simulated Raman spectrum of Aβ42 after the interaction with the liposome as predicted by MD; simulated Raman spectrum of Aβ42 after the interaction with the lipodisc as predicted by MD; experimental Raman spectrum of Aβ42 after 24 h in water. Figures 11(b), respectively 11(c), compare experimental and calculated Raman spectra for the structures of Aβ42 in the liposome, respectively the lipodisc.

To obtain the theoretical Raman spectrum of Aβ42 in water (see Aβ42 NMR CTTM in Figure 11a), we use the PDB molecular structure that is transitional between α-helix and β-turn conformations (code 6SZF) measured by NMR in 50% HFIP and 50% water solutions (Santoro et al., 2021). We choose this structure because it closely correlates with the early stage of Alzheimer's disease, and thus is crucial for unveiling mechanisms of its progression and developing efficient early detection protocols and therapies. Figure 11(a) also depicts the experimental Raman spectra of Aβ42 measured after 0 h and 24 h of peptide dissolution in pure water. It is seen from the figure that the experimental Raman spectra are in a good agreement with the CTTM calculated ones. Since the NMR Aβ42 structure represents the early stage of conformational transformation, it is reasonable to observe that the theoretical vibrational bands in the Amide I region (1600–1800 cm^{-1}) of the NMR amyloid spectrum correlate stronger with the experiment performed immediately after dissolution of Aβ molecules in water. It should be noted that we do not expect to achieve a complete correspondence here between our CTTM calculations for the NMR Aβ structure and Raman measurements in water, because this would require the utilization of the same HFIP–water medium or another molecular structure from the PDB database. The former strategy is irrelevant in terms of repeating the physiological conditions for studying Alzheimer's disease progression, while the latter is impossible due to the lack of NMR Aβ studies in pure water.

At this stage of our research, we correlate the vibrational modes obtained theoretically for the NMR Aβ structure with those observed in experiments at the initial stage of peptide dissolution in water (Figure 11 and Table S1). The obtained

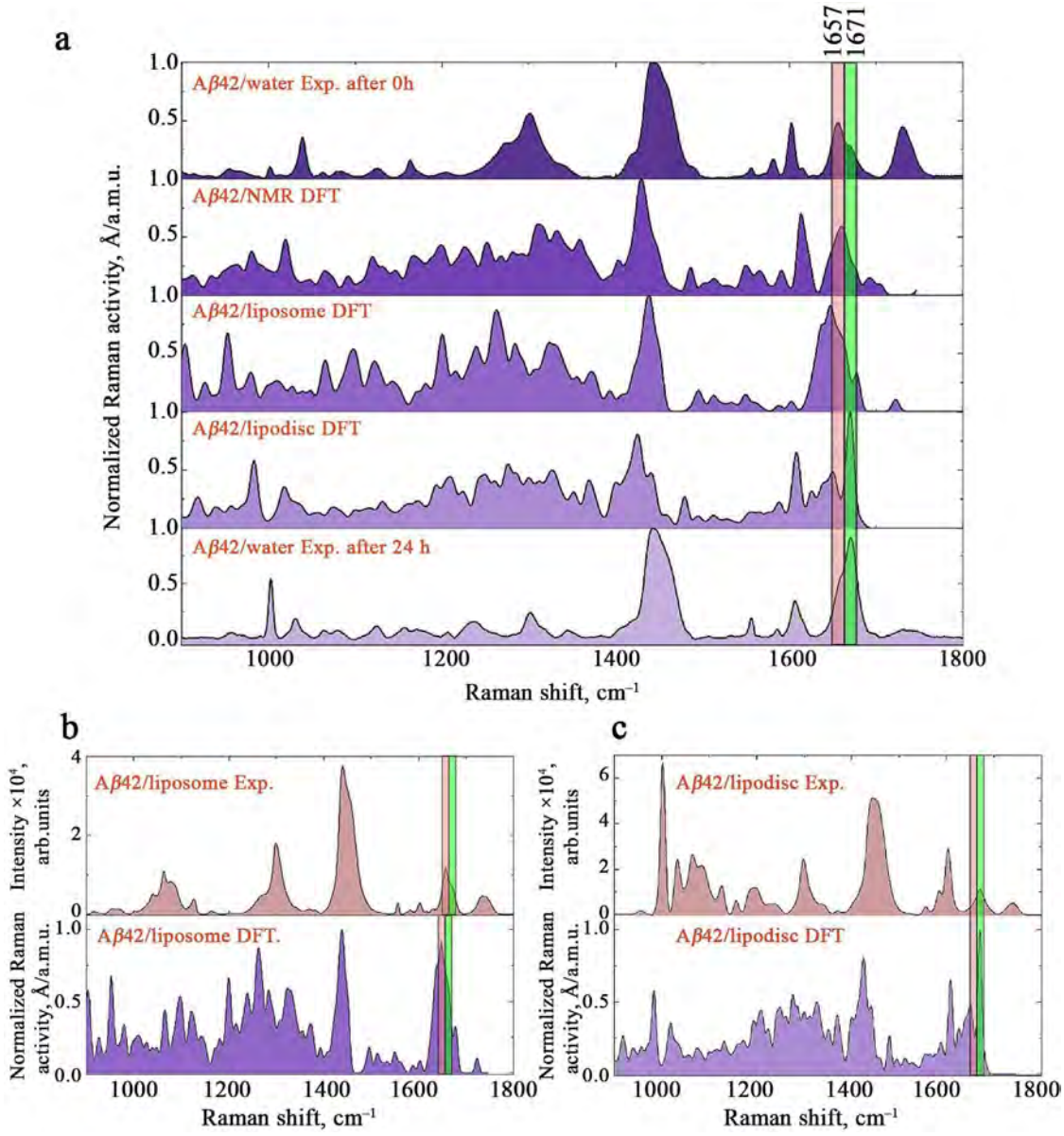

Figure 11. (a) Raman spectra for different Aβ42 systems. Experimental and calculated Raman spectra for Aβ42 after interaction with (b) liposome and (c) lipodisc.

results show that most experimental vibrational bands located in the amide I, amide II, and extended amide III regions, are reasonably well reproduced by the CTTM DFT method. Nevertheless, some differences are noticeable: we calculate 1677 and 1694 cm^{-1} vibrational modes in Amide I region after scaling, while the measurements reveal the same modes at 1657 and 1677 cm^{-1} for Raman shifts. We may connect this discrepancy with the harmonic approximation underlying DFT calculations of Raman spectra, which sets the uncertainty range for the amide I region within approximately 100 cm^{-1} of Raman shifts (Kubelka & Keiderling, 2001). This uncertainty can be partially reduced by accounting for the environment, which is done in this work. Besides, a common practice to enhance the calculation agreement with experiments is to apply carefully chosen scaling factors (Merrick et al., 2007; A. P. Scott & Radom, 1996; Sinha et al., 2004). However, it has been previously demonstrated (Kubelka & Keiderling, 2001) that even with the utilization of these approaches, Raman vibrational modes in the Amide I region are usually overestimated compared to experimental values. This is attributed to the incorrect DFT prediction of the C = O bond length in molecules (Kubelka & Keiderling, 2001; Torii et al., 1998).

Figure 11 and Table S1 also show that the CTTM approach provides a modest reproducibility of vibrational frequencies in the amide III spectral region when compared to the experiment. For example, the calculated spectrum depicts additional vibrational bands at 1237, 1265, 1327, and 1373 cm^{-1}, which are not detected in experiments. Moreover, there is a significant difference in the Raman scattering activity of coinciding bands. We cannot attribute these errors solely to the harmonic approximation. We assume that this is the result of the interplay between inherent errors in DFT and CTTM, as we demonstrated when verifying the accuracy of CTTM.

Based on the obtained results and understanding of possible sources for the detected discrepancy between calculations and experiments, we can cautiously conclude that the

Aβ42 conformation in water at the initial stage of dissolution is transitional from α-helical to β-turn/random coil. Significantly, these results also suggest the robustness of the CTTM approach for investigating the vibrational dynamics of large polypeptide structures. Therefore, it is tempting to apply CTTM for the investigations of more complex situations, such as Aβ42 conformation changes caused by interaction with liposomes or lipodiscs.

CCTM calculations for Aβ42 after the interaction with liposome or lipodisc. Figures 11(b), respectively 11(c) compare experimental Raman spectra with CTTM calculations for Aβ42 after the interaction with liposome, respectively lipodisc. To obtain CTTM Raman spectra in this case, we use the Aβ42 structure obtained by MD simulations (Figures 10b,d). Figure 11 shows that all characteristic Raman modes and corresponding activities are accurately reproduced by the CTTM approach. However, aiming the investigation of the Aβ42 conformational state, we focus only on the extended amide I region. The CTTM approach predicted the vibrational modes at 1649, 1662, and 1651 cm^{-1}, 1671 cm^{-1} after scaling for the MD Aβ structure after the interaction with the liposome and lipodisc, respectively. Following a common notation (Bunaciu et al., 2015), the mode at a lower Raman shift (1649 and 1651 cm^{-1}) is attributed to the α-helical conformation, while the mode at a larger shift (1662 and 1671 cm^{-1}) is attributed to the β-turn/random coil.

Figure 11 also reveals the variation in Raman activities of these bands: α-helical vibration mode dominates the Raman spectrum of Aβ in the liposome, while the interaction of Aβ42 with the lipodisc leads to the β–turn/random coil conformation. Significantly, the same changes are observed in experimental Raman spectra, indicating the possibility of using theoretical results (MD and DFT) to reveal the mechanisms responsible for the conformation change of Aβ42 molecules in different environments.

4. Conclusion

In summary, we have conducted an experimental study on the conformational dynamics of Aβ42 in water and its interaction with lipid membrane mimetics using Raman spectroscopy. Our findings have indicated that the secondary structure of Aβ42 in liposomes is dominated by the time-stable α-helix conformation. Interestingly, yet we have expected to observe the same peptide conformation presented in lipodisc, it has surprisingly been revealed to turn to the β-turn/random coil. These experimental findings have been validated by the MD and DFT simulations, demonstrating good agreement. The copolymer surrounding the lipodisc-peptide system has been interpreted as causing ordering in the carboxyl chains of the bilayer, which in turn affects the secondary structure of the Aβ42 peptide.

Although comparisons between proteomic compound conformations in mimetics and real structures should be made with caution, the results of the Raman study have shown that Aβ42 peptides presented in liposomes maintain their native form, unlike lipodiscs. The copolymer affects the lipid bilayer, altering its conformation and preventing the peptide from maintaining its original structure. In the future, it is recommended that the SMA copolymer should not be used in lipid-protein systems when characterizing peptides that are sensitive to conformational changes.

Therefore, the combination of insights from MD, DFT, and Raman studies is a promising and reliable approach to provide a more complete understanding of the physicochemical processes occurring in living organisms. This conclusion is based on the high correlation observed between experimental data and theoretical modeling, both for simple systems such as Aβ molecules in water and for more complex interactions of peptide molecules with artificial cellular components in the form of lipodiscs. This combination allows monitoring of process products and provides insight into their mechanisms. It also enables theoretical prediction of results for complex biological processes without the need for expensive experimental facilities.

Acknowledgements

The authors have benefited from much useful access to the HybriLIT heterogeneous computing platform, kindly provided by MLIT, JINR.

Disclosure statement

No potential conflict of interest was reported by the authors.

Funding

This work was supported by the JINR project 'Nanobiophotonics' (# 1147-1), grant for collaboration between the Joint Institute for Nuclear Research, Dubna, Russia and Serbia (JINR-Serbia_P7, 2023), and grant of the Belarusian Republican Foundation for Fundamental Research (# T22PIIM-007).

ORCID

Kahramon Mamatkulov http://orcid.org/0000-0001-7503-9362
Siarhei Zavatski http://orcid.org/0000-0003-4530-4545
Yersultan Arynbek http://orcid.org/0000-0002-6942-8211
Heba A. Esawii http://orcid.org/0000-0002-0638-9411
Aliaksandr Burko http://orcid.org/0000-0003-1097-1129
Hanna Bandarenka http://orcid.org/0000-0003-4254-8261
Grigory Arzumanyan http://orcid.org/0000-0002-8755-0747

Data availability statement

Data available on request from the authors.

References

Abraham, M. J., Murtola, T., Schulz, R., Páll, S., Smith, J. C., Hess, B., & Lindah, E. (2015). Gromacs: High performance molecular simulations through multi-level parallelism from laptops to supercomputers. *SoftwareX*, *1–2*, 19–25. https://doi.org/10.1016/j.softx.2015.06.001

Allen, M. P., & Tildesley, D. J. (1989). Computer Simulation of Liquids (Oxford Science Publications) SE - Oxford science publications. *In Oxford University Press* (Vol. 45).

Barron, L. D. (2004). Molecular light scattering and optical activity. In *Molecular light scattering and optical activity*. https://doi.org/10.1017/cbo9780511535468

Becke, A. D. (1993). A new mixing of Hartree-Fock and local density-functional theories. *The Journal of Chemical Physics*, *98*(2), 1372–1377. https://doi.org/10.1063/1.464304

Berhanu, W. M., Mikhailov, I. A., & Masunov, A. E. (2010). Are density functional theory predictions of the Raman spectra accurate enough to distinguish conformational transitions during amyloid formation? *Journal of Molecular Modeling*, *16*(6), 1093–1101. https://doi.org/10.1007/s00894-009-0610-2

Berkowitz, M. L. (2009). Detailed molecular dynamics simulations of model biological membranes containing cholesterol. *Biochimica Et Biophysica Acta*, *1788*(1), 86–96. https://doi.org/10.1016/j.bbamem.2008.09.009

Berman, H. M., Westbrook, J., Feng, Z., Gilliland, G., Bhat, T. N., Weissig, H., Shindyalov, I. N., & Bourne, P. E. (2000). The protein data bank. *Nucleic Acids Research*, *28*(1), 235–242. https://doi.org/10.1093/nar/28.1.235

Bieler, N. S., Haag, M. P., Jacob, C. R., & Reiher, M. (2011). Analysis of the Cartesian Tensor Transfer Method for calculating vibrational spectra of polypeptides. *Journal of Chemical Theory and Computation*, *7*(6), 1867–1881. https://doi.org/10.1021/ct2001478

Bokvist, M., Lindström, F., Watts, A., & Gröbner, G. (2004). Two types of Alzheimer's b-amyloid (1–40) peptide membrane interactions: aggregation preventing transmembrane anchoring versus accelerated surface fibril formation. *Journal of Molecular Biology*, *335*(4), 1039–1049. https://doi.org/10.1016/j.jmb.2003.11.046

Born, M., & Oppenheimer, R. (1927). Zur Quantentheorie der Molekeln. *Annalen Der Physik*, *389*(20), 457–484. https://doi.org/10.1002/andp.19273892002

Bouř, P., & Keiderling, T. A. (2002). Partial optimization of molecular geometry in normal coordinates and use as a tool for simulation of vibrational spectra. *The Journal of Chemical Physics*, *117*(9), 4126–4132. https://doi.org/10.1063/1.1498468

Bouř, P., Kapitán, J., & Baumruk, V. (2001). Simulation of the Raman optical activity of L-alanyl-L-alanine. *The Journal of Physical Chemistry A*, *105*(26), 6362–6368. https://doi.org/10.1021/jp002572b

Bouř, P., Sopková, J., BednáRová, L., Maloň, P., & Keiderling, T. A. (1997). Transfer of molecular property tensors in cartesian coordinates: A new algorithm for simulation of vibrational spectra. *Journal of Computational Chemistry*, *18*(5), 646–659. https://doi.org/10.1002/(SICI)1096-987X(19970415)18:5<646::AID-JCC6>3.0.CO;2-N

Bouř, P., ZáRuba, K., Urbanová, M., Setnička, V., Matějka, P., Fiedler, Z., KráL, V., & Volka, K. (2000). Vibrational circular dichroism of tetraphenylporphyrin in peptide complexes? A computational study. *Chirality*, *12*(4), 191–198. https://doi.org/10.1002/(SICI)1520-636X(2000)12:4<191::AID-CHIR5>3.0.CO;2-W

Bunaciu, A. A., Aboul-Enein, H. Y., & Hoang, V. D. (2015). Raman spectroscopy for protein analysis. *In Applied Spectroscopy Reviews*, *50*(5), 377–386. https://doi.org/10.1080/05704928.2014.990463

Bunow, M. R., & Levin, I. W. (1977). Raman spectra and vibrational assignments for deuterated membrane lipids. 1,2-Dipalmitoyl phosphatidylcholine-d9 and -d62. *Biochimica Et Biophysica Acta (BBA) - Lipids and Lipid Metabolism*, *489*(2), 191–206. https://doi.org/10.1016/0005-2760(77)90138-2

Burke, K. (2012). Perspective on density functional theory. *The Journal of Chemical Physics*, *136*(15), 150901. https://doi.org/10.1063/1.4704546

Bush, S. F., Adams, R. G., & Levin, I. W. (1980). Structural reorganizations in lipid bilayer systems: Effect of hydration and sterol addition on Raman spectra of dipalmitoylphosphatidylcholine multilayers. *Biochemistry*, *19*(19), 4429–4436. https://doi.org/10.1021/bi00560a008

Case, D. A., Cheatham, T. E., Darden, T., Gohlke, H., Luo, R., Merz, K. M., Onufriev, A., Simmerling, C., Wang, B., & Woods, R. J. (2005). The Amber biomolecular simulation programs. In *Journal of computational chemistry* (Vol. 26, Issue 16, pp. 1668–1688). John Wiley & Sons, Ltd. https://doi.org/10.1002/jcc.20290

Chen, G. F., Xu, T. H., Yan, Y., Zhou, Y. R., Jiang, Y., Melcher, K., & Xu, H. E. (2017). Amyloid beta: Structure, biology and structure-based therapeutic development. *Acta Pharmacologica Sinica*, *38*(9), 1205–1235. https://doi.org/10.1038/aps.2017.28

Chorev, D. S., & Robinson, C. V. (2020). The importance of the membrane for biophysical measurements. *Nature Chemical Biology*, *16*(12), 1285–1292. https://doi.org/10.1038/s41589-020-0574-1

Cohen, A. S., & Calkins, E. (1959). Electron microscopic observations on a fibrous component in amyloid of diverse origins. *Nature*, *183*(4669), 1202–1203. https://doi.org/10.1038/1831202a0

Cole, D. J., & Hine, N. D. M. (2016). Applications of large-scale density functional theory in biology. *Journal of Physics: Condensed Matter*, *28*(39), 393001. https://doi.org/10.1088/0953-8984/28/39/393001

Collins, M. A., & Bettens, R. P. A. (2015). Energy-based molecular fragmentation methods. *Chemical Reviews*, *115*(12), 5607–5642. https://doi.org/10.1021/cr500455b

Craig, A. F., Clark, E. E., Sahu, I. D., Zhang, R., Frantz, N. D., Al-Abdul-Wahid, M. S., Dabney-Smith, C., Konkolewicz, D., & Lorigan, G. A. (2016). Tuning the size of styrene-maleic acid copolymer-lipid nanoparticles (SMALPs) using RAFT polymerization for biophysical studies. *Biochimica Et Biophysica Acta*, *1858*(11), 2931–2939. https://doi.org/10.1016/j.bbamem.2016.08.004

Crescenzi, O., Tomaselli, S., Guerrini, R., Salvadori, S., D'Ursi, A. M., Temussi, P. A., & Picone, D. (2002). Solution structure of the Alzheimer amyloid β-peptide (1-42) in an apolar microenvironment: Similarity with a virus fusion domain. *European Journal of Biochemistry*, *269*(22), 5642–5648. https://doi.org/10.1046/j.1432-1033.2002.03271.x

D'Imprima, E., Floris, D., Joppe, M., Sánchez, R., Grininger, M., & Kühlbrandt, M. (2019). Protein denaturation at the air-water interface and how to prevent it. *eLife*, *8*, e42747. https://doi.org/10.7554/eLife.42747

DeLano, W. L. (2020). The PyMOL Molecular Graphics System, Version 2.3. *In Schrödinger LLC*.

Dörr, J. M., Scheidelaar, S., Koorengevel, M. C., Dominguez, J. J., Schäfer, M., van Walree, C. A., & Killian, J. A. (2016). The styrene–maleic acid copolymer: A versatile tool in membrane research. *European Biophysics Journal*, (*45*(1), 3–21. https://doi.org/10.1007/s00249-015-1093-y

Efremov, R., Nolde, D., Konshina, A., Syrtcev, N., & Arseniev, A. (2012). Peptides and proteins in membranes: What can we learn via computer simulations? *Current Medicinal Chemistry*, *11*(18), 2421–2442. https://doi.org/10.2174/0929867043364496

Fasanella, A., Cosentino, K., Beneduci, A., Chidichimo, G., Cazzanelli, E., Barberi, R. C., & Castriota, M. (2018). Thermal structural evolutions of DMPC-water biomimetic systems investigated by Raman Spectroscopy. *Biochimica Et Biophysica Acta. Biomembranes*, *1860*(6), 1253–1258. https://doi.org/10.1016/j.bbamem.2018.02.021

Gordon, M. S., Fedorov, D. G., Pruitt, S. R., & Slipchenko, L. V. (2012). Fragmentation methods: A route to accurate calculations on large systems. *Chemical Reviews*, *112*(1), 632–672. https://doi.org/10.1021/cr200093j

Grahnen, J. A., Amunson, K. E., & Kubelka, J. (2010). DFT-based simulations of IR amide I′. *The Journal of Physical Chemistry. B*, *114*(40), 13011–13020. https://doi.org/10.1021/jp106639s

Gumbart, J., Wang, Y., Aksimentiev, A., Tajkhorshid, E., & Schulten, K. (2005). Molecular dynamics simulations of proteins in lipid bilayers. *Current Opinion in Structural Biology*, *15*(4), 423–431. https://doi.org/10.1016/j.sbi.2005.07.007

Harrison, R. S., Sharpe, P. C., Singh, Y., & Fairlie, D. P. (2007). Amyloid peptides and proteins in review. *Reviews of Physiology, Biochemistry and Pharmacology*, *159*, 1–77.). https://doi.org/10.1007/112_2007_0701

Herrmann, C., & Reiher, M. (2006). First-principles approach to vibrational spectroscopy of biomolecules. In *Atomistic approaches in modern biology* (Vol. 268, pp. 85–132). Springer. https://doi.org/10.1007/128_2006_082

Huang, J., Rauscher, S., Nawrocki, G., Ran, T., Feig, M., De Groot, B. L., Grubmüller, H., & MacKerell, A. D. (2016). CHARMM36m: An improved force field for folded and intrinsically disordered proteins. *Nature Methods*, *14*(1), 71–73. https://doi.org/10.1038/nmeth.4067

Huang, R., Setnicka, V., Etienne, M. A., Kim, J., Kubelka, J., Hammer, R. P., & Keiderling, T. A. (2007). Cross-strand coupling of a β-hairpin peptide stabilized with an Aib-Gly turn studied using isotope-edited IR spectroscopy. *Journal of the American Chemical Society*, *129*(44), 13592–13603. https://doi.org/10.1021/ja0736414

Hudecová, J., Kapitán, J., Baumruk, V., Hammer, R. P., Keiderling, T. A., & Bour, P. (2010). Side chain and flexibility contributions to the Raman optical activity spectra of a model cyclic hexapeptide. *The Journal of Physical Chemistry. A*, *114*(28), 7642–7651. https://doi.org/10.1021/jp104744a

Humphrey, W., Dalke, A., & Schulten, K. (1996). VMD: Visual molecular dynamics. *Journal of Molecular Graphics*, *14*(1), 33–38. https://doi.org/10.1016/0263-7855(96)00018-5

Jo, S., Cheng, X., Islam, S. M., Huang, L., Rui, H., Zhu, A., Lee, H. S., Qi, Y., Han, W., Vanommeslaeghe, K., MacKerell, A. D., Roux, B., & Im, W. (2014). CHARMM-GUI PDB manipulator for advanced modeling and simulations of proteins containing nonstandard residues. *Advances in Protein Chemistry and Structural Biology*, *96*, 235–265. https://doi.org/10.1016/bs.apcsb.2014.06.002

Jo, S., Kim, T., & Im, W. (2007). Automated builder and database of protein/membrane complexes for molecular dynamics simulations. *PLoS One*, *2*(9), e880. https://doi.org/10.1371/journal.pone.0000880

Jo, S., Kim, T., Iyer, V. G., & Im, W. (2008). CHARMM-GUI: A web-based graphical user interface for CHARMM. *Journal of Computational Chemistry*, *29*(11), 1859–1865. https://doi.org/10.1002/jcc.20945

Jo, S., Lim, J. B., Klauda, J. B., & Im, W. (2009). CHARMM-GUI membrane builder for mixed bilayers and its application to yeast membranes. *Biophysical Journal*, *97*(1), 50–58. https://doi.org/10.1016/j.bpj.2009.04.013

Kapitán, J., Baumruk, V., & Bour, P. (2006). Demonstration of the ring conformation in polyproline by the Raman optical activity. *Journal of the American Chemical Society*, *128*(7), 2438–2443. https://doi.org/10.1021/ja057337r

Kapitán, J., Zhu, F., Hecht, L., Gardiner, J., Seebach, D., & Barron, L. D. (2008). Solution structures of β peptides from raman optical activity. *Angewandte Chemie*, *120*(34), 6492–6494. https://doi.org/10.1002/ange.200801111

Kessler, J., Kapitán, J., & Bouř, P. (2015). First-principles predictions of vibrational raman optical activity of globular proteins. *The Journal of Physical Chemistry Letters*, *6*(16), 3314–3319. https://doi.org/10.1021/acs.jpclett.5b01500

Khandelia, H., Ipsen, J. H., & Mouritsen, O. G. (2008). The impact of peptides on lipid membranes. *Biochimica Et Biophysica Acta*, (*1778*(7-8), 1528–1536. https://doi.org/10.1016/j.bbamem.2008.02.009

Killian, J. A., & Nyholm, T. K. (2006). Peptides in lipid bilayers: The power of simple models. *Current Opinion in Structural Biology*, *16*(4), 473–479. https://doi.org/10.1016/j.sbi.2006.06.007

Klamt, A., Jonas, V., Bürger, T., & Lohrenz, J. C. W. (1998). Refinement and parametrization of COSMO-RS. *The Journal of Physical Chemistry A*, *102*(26), 5074–5085. https://doi.org/10.1021/jp980017s

Kohn, W., & Sham, L. J. (1965). Self-consistent equations including exchange and correlation effects. *Physical Review*, *140*(4A), A1133–A1138. https://doi.org/10.1103/PhysRev.140.A1133

Kubelka, J., & Keiderling, T. A. (2001). Ab initio calculation of amide carbonyl stretch vibrational frequencies in solution with modified basis sets. 1. JV-methyl acetamide. *The Journal of Physical Chemistry A*, *105*(48), 10922–10928. https://doi.org/10.1021/jp013203y

Kubelka, J., & Keiderling, T. A. (2001). The anomalous infrared amide I intensity distribution in 13C isotopically labeled peptide β-sheets comes from extended, multiple-stranded structures. An ab initio study. *Journal of the American Chemical Society*, *123*(25), 6142–6150. https://doi.org/10.1021/ja010270x

Leach, A. R. (2001). Molecular modeling: Principles and applications (2nd ed., pp. 234–247). Prentice Hall.

Lee, C., Yang, W., & Parr, R. G. (1988). Development of the Colle-Salvetti correlation-energy formula into a functional of the electron density. *Physical Review. B, Condensed Matter*, *37*(2), 785–789. https://doi.org/10.1103/PhysRevB.37.785

Majeed, S., Ahmad, A. B., Sehar, U., & Georgieva, E. R. (2021). Lipid membrane mimetics in functional and structural studies of integral membrane proteins. In. *Membranes*, *11*(9), 685. https://doi.org/10.3390/membranes11090685

Marino, T., Russo, N., Toscano, M., & Pavelka, M. (2010). On the metal ion (Zn^{2+}, Cu^{2+}) coordination with beta-amyloid peptide: DFT computational study. *Interdisciplinary Sciences, Computational Life Sciences*, *2*(1), 57–69. https://doi.org/10.1007/s12539-010-0086-x

Mazaleyrat, J. P., Wright, K., Gaucher, A., Wakselman, M., Oancea, S., Formaggio, F., Toniolo, C., Setnička, V., Kapitán, J., & Keiderling, T. A. (2003). Synthesis and conformational study of homo-peptides based on (S)-Bin, a C2-symmetric binaphthyl-derived Cα,α-disubstituted glycine with only axial chirality. *Tetrahedron: Asymmetry*, *14*(13), 1879–1893. https://doi.org/10.1016/S0957-4166(03)00285-4

Mennucci, B., Cappelli, C., Cammi, R., & Tomasi, J. (2011). Modeling solvent effects on chiroptical properties. *In Chirality*, *23*(9), 717–729. https://doi.org/10.1002/chir.20984

Mensch, C., Bultinck, P., & Johannessen, C. (2019). The effect of protein backbone hydration on the amide vibrations in Raman and Raman optical activity spectra. *Physical Chemistry Chemical Physics: PCCP*, *21*(4), 1988–2005. https://doi.org/10.1039/c8cp06423g

Merrick, J. P., Moran, D., & Radom, L. (2007). An evaluation of harmonic vibrational frequency scale factors. *The Journal of Physical Chemistry. A*, *111*(45), 11683–11700. https://doi.org/10.1021/jp073974n

Mezei, M., & Jedlovszky, P. (2007). *Statistical thermodynamics through computer simulation to characterize phospholipid interactions in membranes* (pp. 127–144). Humana Press. https://doi.org/10.1007/978-1-59745-519-0_9

Nafie, L. A. (2011). Vibrational Optical Activity: Principles and Applications. In *Vibrational Optical Activity: Principles and Applications*. https://doi.org/10.1002/9781119976516

Neese, F. (2012). The ORCA program system. *WIREs Computational Molecular Science*, *2*(1), 73–78. https://doi.org/10.1002/wcms.81

Neese, F., Wennmohs, F., Becker, U., & Riplinger, C. (2020). The ORCA quantum chemistry program package. *The Journal of Chemical Physics*, *152*(22) https://doi.org/10.1063/5.0004608

Niu, Z., Zhang, Z., Zhao, W., & Yang, J. (2018). Interactions between amyloid β peptide and lipid membranes. *Biochimica Et Biophysica Acta. Biomembranes*, *1860*(9), 1663–1669. https://doi.org/10.1016/j.bbamem.2018.04.004

Parr, R. G. (1980). Density functional theory of atoms and molecules. In *Horizons of quantum chemistry* (pp. 5–15). https://doi.org/10.1007/978-94-009-9027-2_2

Perdew, J. P., Burke, K., & Wang, Y. (1996). Generalized gradient approximation for the exchange-correlation hole of a many-electron system. *Physical Review. B, Condensed Matter*, *54*(23), 16533–16539. https://doi.org/10.1103/PhysRevB.54.16533

Pettersen, E. F., Goddard, T. D., Huang, C. C., Couch, G. S., Greenblatt, D. M., Meng, E. C., & Ferrin, T. E. (2004). UCSF Chimera: A visualization system for exploratory research and analysis. *Journal of Computational Chemistry*, *25*(13), 1605–1612. https://doi.org/10.1002/jcc.20084

Picone, P., Nuzzo, D., Giacomazza, D., & Di Carlo, M. (2020). *β*-Amyloid peptide: The cell compartment multi-faceted interaction in Alzheimer's disease. *Neurotoxicity Research*, *37*(2), 250–263. https://doi.org/10.1007/s12640-019-00116-9

Polavarapu, P. L. (1990). Ab initio vibrational Raman and Raman optical activity spectra. *The Journal of Physical Chemistry*, *94*(21), 8106–8112. https://doi.org/10.1021/j100384a024

Poojari, C., Kukol, A., & Strodel, B. (2013). How the amyloid-β peptide and membranes affect each other: An extensive simulation study. *Biochimica Et Biophysica Acta*, *1828*(2), 327–339. https://doi.org/10.1016/j.bbamem.2012.09.001

Raghavachari, K., & Saha, A. (2015). Accurate composite and fragment-based quantum chemical models for large molecules. *Chemical Reviews*, (*115*(12), 5643–5677. https://doi.org/10.1021/cr500606e

Sakono, M., & Zako, T. (2010). Amyloid oligomers: Formation and toxicity of Aβ oligomers. *In FEBS Journal*, *277*(6), 1348–1358. https://doi.org/10.1111/j.1742-4658.2010.07568.x

Santoro, A., Grimaldi, M., Buonocore, M., Stillitano, I., & D'Ursi, A. M. (2021). Exploring the early stages of the amyloid aβ(1–42) peptide aggregation process: An NMR study. *Pharmaceuticals*, *14*(8). https://doi.org/10.3390/ph14080732

Scott, A. P., & Radom, L. (1996). Harmonic vibrational frequencies: An evaluation of Hartree-Fock, Møller-Plesset, quadratic configuration interaction, density functional theory, and semiempirical scale factors.

The Journal of Physical Chemistry, *100*(41), 16502–16513. https://doi.org/10.1021/jp960976r

Scott, H. L. (2002). Modeling the lipid component of membranes. *Current Opinion in Structural Biology*, *12*(4), 495–502. https://doi.org/10.1016/S0959-440X(02)00353-6

Sebek, J., Kapitán, J., Sebestík, J., Baumruk, V., & Bour, P. (2009). L-alanyl-l-alanine conformational changes induced by pH As monitored by the Raman optical activity spectra. *The Journal of Physical Chemistry. A*, *113*(27), 7760–7768. https://doi.org/10.1021/jp902739r

Sholl, D. S., & Steckel, J. A. (2009). Density Functional Theory: A Practical Introduction. In *John Wiley and Sons*. John Wiley and Sons. https://doi.org/10.1002/9780470447710

Sinha, P., Boesch, S. E., Gu, C., Wheeler, R. A., & Wilson, A. K. (2004). Harmonic vibrational frequencies: Scaling factors for HF, B3LYP, and MP2 methods in combination with correlation consistent basis sets. *The Journal of Physical Chemistry A*, *108*(42), 9213–9217. https://doi.org/10.1021/jp048233q

Spiker, R. C., & Levin, I. W. (1975). Raman spectra and vibrational assignments for dipalmitoyl phosphatidylcholine and structurally related molecules. *Biochimica Et Biophysica Acta*, *388*(3), 361–373. https://doi.org/10.1016/0005-2760(75)90095-8

Stelzmann, R. A., Norman Schnitzlein, H., & Reed Murtagh, F. (1995). An english translation of alzheimer's 1907 paper, "über eine eigenartige erkankung der hirnrinde". *Clinical Anatomy*, *8*(6), 429–431. https://doi.org/10.1002/ca.980080612

Straub, J. E., & Thirumalai, D. (2014). Membrane–protein interactions are key to understanding amyloid formation. *The Journal of Physical Chemistry Letters*, *5*(3), 633–635. https://doi.org/10.1016/j.bbamem.2018.04.004

Torii, H., Tatsumi, T., & Tasumi, M. (1998). Effects of hydration on the structure, vibrational wavenumbers, vibrational force field and resonance raman intensities of n-methylacetamide. *Journal of Raman Spectroscopy*, *29*(6), 537–546. https://doi.org/10.1002/(sici)1097-4555(199806)29:6

Vargas, C., Arenas, R. C., Frotscher, E., & Keller, S. (2015). Nanoparticle self-assembly in mixtures of phospholipids with styrene/maleic acid copolymers or fluorinated surfactants. *Nanoscale*, *7*(48), 20685–20696. https://doi.org/10.1039/c5nr06353a

Vigh, L., Escribá, P. V., Sonnleitner, A., Sonnleitner, M., Piotto, S., Maresca, B., Horváth, I., & Harwood, J. L. (2005). The significance of lipid composition for membrane activity: New concepts and ways of assessing function. *Progress in Lipid Research*, *44*(5), 303–344. https://doi.org/10.1016/j.plipres.2005.08.001

Wheatley, M., Charlton, J., Jamshad, M., Routledge, S. J., Bailey, S., La-Borde, P. J., Azam, M. T., Logan, R. T., Bill, R. M., Dafforn, T. R., & Poyner, D. R. (2016). GPCR-styrene maleic acid lipid particles (GPCR-SMALPs): Their nature and potential. *Biochemical Society Transactions*, *44*(2), 619–623. https://doi.org/10.1042/BST20150284

Wong, P. T., Schauerte, J. A., Wisser, K. C., Ding, H., Lee, E. L., Steel, D. G., & Gafni, A. (2009). Amyloid-β membrane binding and permeabilization are distinct processes influenced separately by membrane charge and fluidity. *Journal of Molecular Biology*, *386*(1), 81–96. https://doi.org/10.1016/j.jmb.2008.11.060

Wu, E. L., Cheng, X., Jo, S., Rui, H., Song, K. C., Dávila-Contreras, E. M., Qi, Y., Lee, J., Monje-Galvan, V., Venable, R. M., Klauda, J. B., & Im, W. (2014). CHARMM-GUI membrane builder toward realistic biological membrane simulations. *Journal of Computational Chemistry*, (*35*(27), 1997–2004. https://doi.org/10.1002/jcc.23702

Yamamoto, S., Kaminský, J., & Bouř, P. (2012). Structure and vibrational motion of insulin from Raman optical activity spectra. *Analytical Chemistry*, *84*(5), 2440–2451. https://doi.org/10.1021/ac2032436

Yamamoto, S., Straka, M., Watarai, H., & Bour, P. (2010). Formation and structure of the potassium complex of valinomycin in solution studied by Raman optical activity spectroscopy. *Physical Chemistry Chemical Physics: PCCP*, *12*(36), 11021–11032. https://doi.org/10.1039/c003277h

Yamamoto, S., Watarai, H., & Bouř, P. (2011). Monitoring the backbone conformation of valinomycin by raman optical activity. *Chemphyschem: A European Journal of Chemical Physics and Physical Chemistry*, *12*(8), 1509–1518. https://doi.org/10.1002/cphc.201000917

Zavatski, S., Bandarenka, H., Hetmańczyk, Ł., Hetmańczyk, J., Vorobyeva, M., Arynbek, Y., Mamatkulov, K., & Arzumanyan, G. (2022). Model phospholipid interaction with cholesterol and melatonin: Raman spectroscopy and density functional theory study. *Journal of Raman Spectroscopy*, *53*(9), 1540–1550. https://doi.org/10.1002/jrs.6409

Zhang, R., Sahu, I. D., Liu, L., Osatuke, A., Comer, R. G., Dabney-Smith, C., & Lorigan, G. A. (2015). Characterizing the structure of lipodisq nanoparticles for membrane protein spectroscopic studies. *Biochimica Et Biophysica Acta*, *1848*(1 Pt B), 329–333. https://doi.org/10.1016/j.bbamem.2014.05.008

Zhu, F., Kapitan, J., Tranter, G. E., Pudney, P. D. A., Isaacs, N. W., Hecht, L., & Barron, L. D. (2008). Residual structure in disordered peptides and unfolded proteins from multivariate analysis and ab initio simulation of Raman optical activity data. *Proteins*, *70*(3), 823–833. https://doi.org/10.1002/prot.21593